Available online at www.sciencedirect.com
SCIENCE DIRECT®
Journal of Catalysis 221 (2004) 178–190
JOURNAL OF CATALYSIS
www.elsevier.com/locate/jcat

Nickel–calcium phosphate/hydroxyapatite catalysts for partial oxidation of methane to syngas: characterization and activation

Jin Hyuk Jun,[a] Tae-Jin Lee,[b] Tae Hoon Lim,[c] Suk-Woo Nam,[c] Seong-Ahn Hong,[c] and Ki June Yoon [a,*]

[a] *Department of Chemical Engineering, Sungkyunkwan University, Suwon 440-746, South Korea*
[b] *School of Chemical Engineering & Technology, Yeungnam University, Kyongsan 712-749, South Korea*
[c] *Battery and Fuel Cell Research Center, Korea Institute of Science and Technology, Seoul 136-791, South Korea*

Received 12 May 2003; revised 16 July 2003; accepted 21 July 2003

Abstract

Nickel–calcium phosphate/hydroxyapatite catalysts exhibited high activity and selectivity in the partial oxidation of methane (POM). Characterizations have been performed in order to understand the characteristics of these catalysts. TEM showed that very fine, needle-shaped nickel particles of a few nanometers were present in the sample after the reaction. TPR showed the presence of three nickel species in the fresh (before-reaction) sample, confirming that the nickel in the calcium hydroxyapatite and phosphate structures comes out as fine particles and is reduced during the reaction. The crystalline phases observed were calcium phosphate, calcium hydroxyapatite, NiO, and metallic Ni. As the Ca/PO_4 ratio increased, the calcium hydroxyapatite phase tended to increase over the calcium phosphate phase. As the Ni/PO_4 ratio increased, the amount of NiO increased in the fresh samples and the amount of metallic Ni also increased in the used (after-reaction) catalysts with the decrease of the NiO. The catalytically active component is certainly the metallic nickel that is produced under reducing environment during the reaction, but its surface is totally reoxidized at 673 K and loses the activity completely. The catalyst could be activated by the reactants only, without the H_2 pretreatment. The first activation could be achieved at 923 K or below, and the subsequent activation at 723 K.

Keywords: Nickel; Partial oxidation of methane; Calcium hydroxyapatite; Calcium phosphate; Syngas

1. Introduction

Hydrogen is regarded as the ultimate clean power source of the future. Its application to fuel cells is a typical example. Catalytic partial oxidation of methane (POM) for synthesis gas and hydrogen production has been an active subject in recent years because it is currently more economical and feasible than other methods such as water electrolysis and photodecomposition. The process arouses renewed interest as a promising alternative to the steam reforming of methane [1–14]. Although the steam reforming of methane is the dominant commercialized process for syngas production, it has some drawbacks relating to the energy and capital costs since it is a highly endothermic reaction and is operated under high pressure. In addition, the water–gas-shift reaction produces significant quantities of carbon dioxide. Compared with the highly endothermic steam reforming, POM is mildly exothermic and does not require high operating pressures and hence is more energy efficient. The reaction can be carried out with lower investment and will produce a smaller amount of CO_2. Recently, POM is of particular interest in fuel processing applications such as in fuel cells for startup from cold, owing to its exothermic nature [3,8]. However, if POM is to be applied to low-temperature fuel cells such as polymer electrolyte membrane fuel cells, subsequent treatments such as conversion of CO to CO_2 by the water–gas-shift reaction and removal of trace CO by the preferential oxidation of CO are required because CO severely poisons the electrode.

There have been numerous studies on POM over various metal catalysts. Ni and noble metals such as Rh, Pt, and Pd are active for POM, and these are usually dispersed on oxide supports. Rh is known to be the most active for

* Corresponding author.
E-mail address: kijyoon@skku.edu (K.J. Yoon).

0021-9517/$ – see front matter
doi:10.1016/j.jcat.2003.07.004

POM [3]. However, Ni is the most extensively studied catalyst because it is effective as well as cheap. Ni is usually supported on alumina and silica, but it is susceptible to the formation of inactive nickel aluminate and silicate. Sintering of Ni and the supports and coke formation are other problems. Several attempts have been reported to overcome these problems. Choudhary et al. [3] have shown that, in supported Ni catalysts prepared by depositing NiO on alumina and silica precoated with MgO, chemical interactions of NiO with the support can be prevented by providing a stable protective layer of magnesium aluminate and silicate. In addition, MgO stabilizes nickel by forming a NiO–MgO solid solution. Hayakawa et al. [7] and Takehira et al. [9] have reported that Ni supported on perovskite-type oxides prepared by solid-phase crystallization, such as $Ni_{0.2}/ATiO_3$ (A: Ca, Sr or Ba), shows good activity and selectivity as well as very low coke formation. They explain that this may be due to highly dispersed and stable Ni metal particles on the perovskite, where the nickel species thermally come out during the reaction from the cations homogeneously distributed in an inert perovskite matrix as the precursor. Takehira [12] has also reported that a Ni/Al–Mg oxide catalyst prepared by solid-phase crystallization, via synthesis of a hydrotalcite (e.g., $Ni_{0.5}Mg_{2.5}Al(OH)_8(CO_3{}^{-2})_{0.5}\cdot 2H_2O$) and its calcination, had very fine Ni particles and showed high activity, selectivity, and stability. Such studies suggest that high dispersion of metal species and/or the use of alkaline earth metals may be beneficial to improve the catalytic performance for the POM. Liu et al. [13,14] have recently reported that $Ni/Ce\text{-}ZrO_2/\theta\text{-}Al_2O_3$ shows high activity and stability and that a protective layer of $Ce\text{-}ZrO_2$ suppresses the formation of inactive $NiAl_2O_4$.

From the work in our laboratory, it has recently been reported that another type of new catalyst, nickel-strontium phosphate, exhibits high activity and selectivity in POM [15–17]. No refractory oxide support was used in this catalyst. It was found that this catalyst could be activated by the reacting gases only (methane + oxygen) at around 850 K. Very fine nickel particles were observed and they are considered to come out from the strontium nickel phosphate and hydroxyapatite structure. Over this catalyst, methane conversion and H_2 and CO concentrations close to or sometimes in excess of those predicted by the thermodynamic equilibrium were observed. This kind of observation has been reported in some earlier works [6,18]. An explanation for this is that the actual catalyst temperature is significantly higher than the temperature usually measured by a thermocouple since the reaction is exothermic. Actually, it has been reported that hot spots in the catalyst bed were detected by an optical pyrometer [6]. On the other hand, it is considered that the presence of Sr imparts some alkalinity to the catalyst and might be beneficial for the suppression of coke formation.

In this work, calcium, in the same group as Sr, was employed instead of strontium, and nickel–calcium phosphate/hydroxyapatite catalysts were investigated for POM as an extension of the previous works. Since nickel–calcium phosphate/hydroxyapatite is a new type of catalyst for POM that has not been investigated by other researchers, characteristics of this material were investigated by several characterization methods. The activation behavior of those catalysts was also studied and compared with that of nickel-strontium phosphate and oxide-supported nickel catalysts.

2. Experimental

2.1. Catalyst preparation

The catalysts were prepared from nearly saturated aqueous solutions of calcium nitrate, nickel nitrate, and dibasic ammonium phosphate. The pH of the solutions was adjusted to 10–11 by adding ammonia water, and predetermined amounts of the solutions were mixed at room temperature with vigorous stirring in 1 h and the water was evaporated to get a thick paste. The mixture was dried at 383 K overnight and finally calcined in air at 1073 K for 2 h to obtain the catalyst. The solid catalyst was crushed and sieved, and the particles of 40- to 80-mesh size were used.

The mole ratio of Ca/PO_4 was varied from 8.0/6 to 10.0/6 and the Ni/PO_4 ratio from 0.5/6 to 3.0/6. The catalysts were designated to be $Ca^*NiP(a)$, where * is 60 times the Ca/PO_4 mole ratio and a is 60 times the Ni/PO_4 mole ratio employed. For example, Ca95NiP(25) has the composition ratio of $Ca_{9.5}Ni_{2.5}(PO_4)_6$. The multiplication by 60 was taken for convenience sake in order to express the composition by integers, since calcium phosphate ($Ca_3(PO_4)_2$) and calcium hydroxyapatite ($Ca_{10}(PO_4)_6(OH)_2$) have the least common multiple of 6 between the subscript numbers of the phosphate group. In addition, -f or -u was affixed when necessary, where f and u denoting fresh (before-reaction) and used (after-reaction) catalyst, respectively.

2.2. Catalyst characterizations

The catalysts were characterized with X-ray diffraction (XRD) using Ni-filtered Cu-K_α (M18xHF-SRA, Mao Science) and high-resolution transmission electron microscopy (HRTEM, JEM3011, JEOL). The temperature-programmed reduction (TPR) was carried out by using 5% H_2/Ar with a ramp rate of 10 K/min for 100 mg of the fresh catalyst. X-ray photoelectron spectroscopy (XPS) measurements were performed using Mg-K_α radiation with the reference of Au $4f_{7/2}$ at 84.00 eV (ESCA 2000). Ni particle sizes were estimated from XRD line broadening analysis using the Scherrer equation. Hydrogen chemisorption experiments were performed with a volumetric adsorption apparatus (Micromeritics ASAP-2000) as well as by employing pulse experiments consisting of repeated injections of a small amount of H_2 in flowing Ar and determination of effluent H_2 by TCD. The hydrogen chemisorption was carried out at room temperature for the fresh samples after reduction by flowing H_2 at 723 K for 2 h and subsequent evacuation

when using the volumetric apparatus or at 1023 K for 2 h and subsequent flushing with Ar when employing the pulse experiment. The amounts of O_2 sorption at 923 K were also measured by employing the pulse experiments for the fresh samples reduced and flushed as described above.

2.3. Performance test

The catalyst performance was tested by a conventional method using an 8-mm i.d. quartz-tube flow reactor. The reaction temperature was measured by a thermocouple directly contacting the catalyst particles and controlled by an electric furnace. Unless specified otherwise, the following standard experimental conditions were employed. The catalyst charge was 0.2 g. The partial pressures of methane and oxygen were 16.2 and 8.1 kPa (0.16 and 0.08 atm), respectively. Ar was used as the diluent gas and the total flow rate was 100 cm^3 (STP)/min. The product gas was analyzed by two gas chromatographs using Carboxen 1004 columns (Supelco); one used Ar as the carrier gas and the other used He. The latter was needed especially when the concentration of produced CO_2 was too low to detect by using the Ar carrier gas. The first reaction experiment for each catalyst was carried out at 673 K by flowing the reaction gas mixture without employing the hydrogen pretreatment.

3. Results and discussion

3.1. TEM results

Fig. 1 shows the TEM pictures for Ca95NiP(25)-f and -u. The used catalyst here is the sample that had experienced a set of reaction experiments in which the reaction temperature was changed from 673 to 1073 K and then down to 673 K with an interval of 50°. As shown later in Section 3.6, the catalyst lost almost all the activity when the temperature was lowered to 673 K.

In the fresh sample, round particles of 5–20 nm in size were observed. These particles were identified as NiO by energy-dispersive X-ray spectroscopy (EDS) equipped in the TEM apparatus, since the major elements in the particles were found to be Ni and O when irradiated with about a 10-nm size beam. At the other part of the catalyst, the major elements were Ca, P, and O, together with a small amount of Ni. In the used sample, very fine particles that had not been seen in the fresh sample were observed. Many of them were in a needle shape, with the width of about 1 nm and the length of several nanometers. Round particles of a few nanometers in diameter were also observed. For these particles a major element was also found to be Ni by EDS. This suggests that the Ni comes out of the matrix during the POM reaction. Similar results had been observed in the previous work on the POM reaction over a Ni-strontium phosphate catalyst [16]. This phenomenon appears similar to the solid-phase crystallization noted in Introduction [9]. Since the used catalyst had been finally exposed to an oxidizing environment of flowing CH_4–O_2 at 673 K for about 1 h where practically no reforming reaction occurred, the nickel surface would have been fully oxidized. In addition, the nickel that had come out did not go back into the matrix but most of it appeared to remain as fine particles. This suggestion of

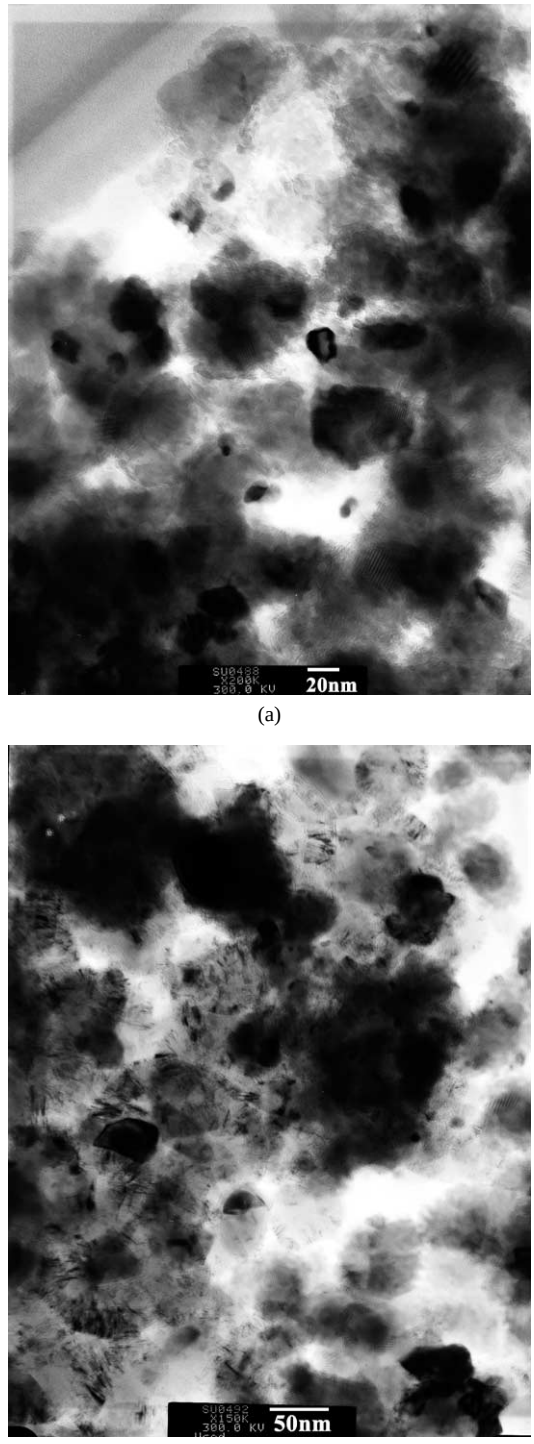

Fig. 1. TEM images of Ca95NiP(25) catalysts. (a) Fresh Ca95NiP(25), (b) used Ca95NiP(25).

the Ni coming out of the matrix will be further examined by XRD and TPR below. One thing to note here is that in the fresh and used samples there may exist very large particles, larger than a 100 nm, but due to the limitation of TEM they would be hard to distinguish from thick parts of the sample.

3.2. XRD analysis

3.2.1. The crystalline phases

The XRD patterns for representative samples are shown in Figs. 2–4. The used samples here are those that had been used for the POM reaction. Each used sample had experienced a set of reaction experiments in which the first experiment was carried out at 1023 K in order to activate the catalyst (see Section 3.6), the next at 1073 K, and the subsequent experiments were carried out by decreasing the temperature with an interval of 50° down to 673 K where the activity usually became near zero. At each temperature the reaction was carried out for about 1 h.

The XRD patterns of some samples of Ca80NiP(a) catalysts are shown in Fig. 2. In these catalysts the calcium hydroxyapatite phase (hexagonal $Ca_{10}(PO_4)_6(OH)_2$; this will be called as the apatite hereafter) was not observed. This is because the Ca/PO_4 mole ratio, 8.0/6, is considerably lower than 10/6 so that it is difficult for the apatite to be formed. Although the Ca/PO_4 ratio was smaller than 9/6, the calcium phosphate phase (hexagonal β-$Ca_3(PO_4)_2$; this will be called as the phosphate hereafter) was well formed.

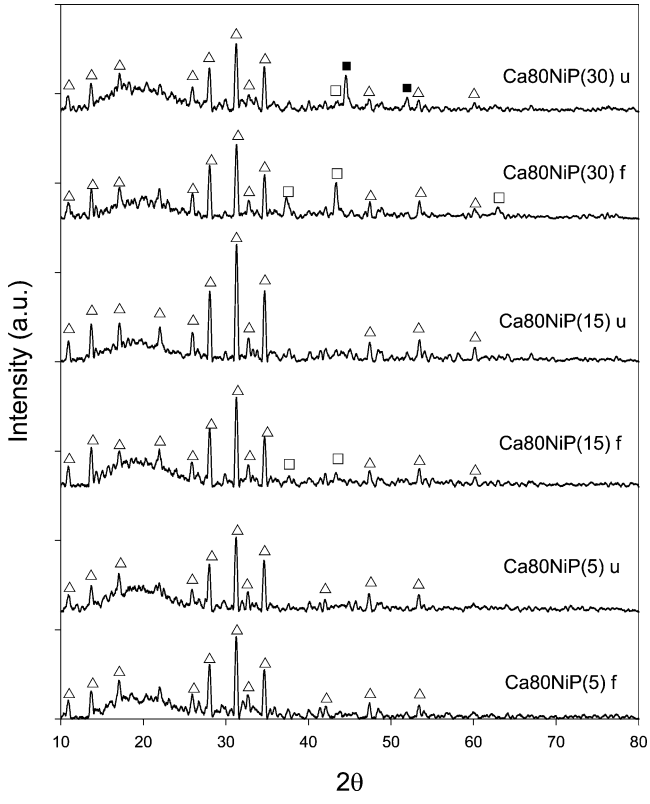

Fig. 2. X-ray diffractograms for Ca80NiP(5), Ca80NiP(15), and Ca80NiP(25) (△, β-$Ca_3(PO_4)_2$; ●, $Ca_{10}(PO_4)_6(OH)_2$; □, NiO; ■, Ni).

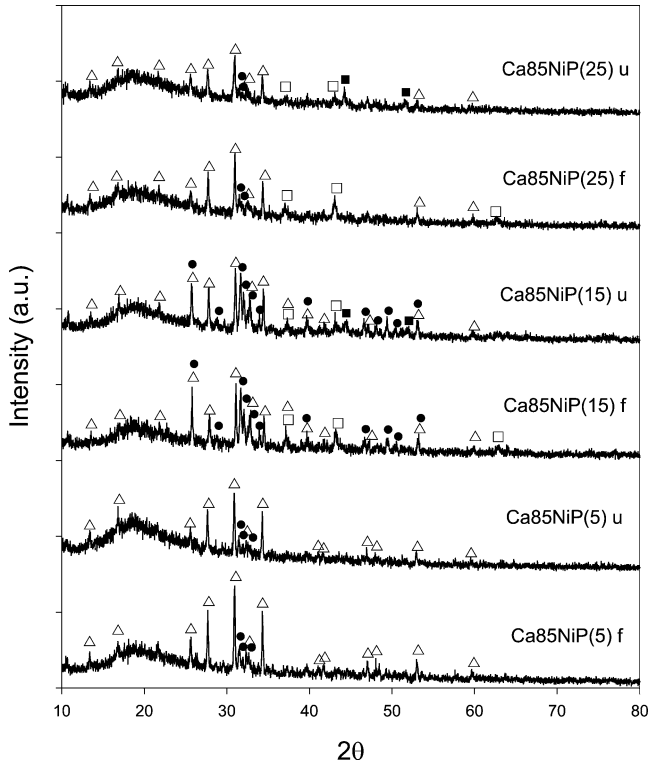

Fig. 3. X-ray diffractograms for Ca85NiP(5), Ca85NiP(15), and Ca85NiP(25) (△, β-$Ca_3(PO_4)_2$; ●, $Ca_{10}(PO_4)_6(OH)_2$; □, NiO; ■, Ni).

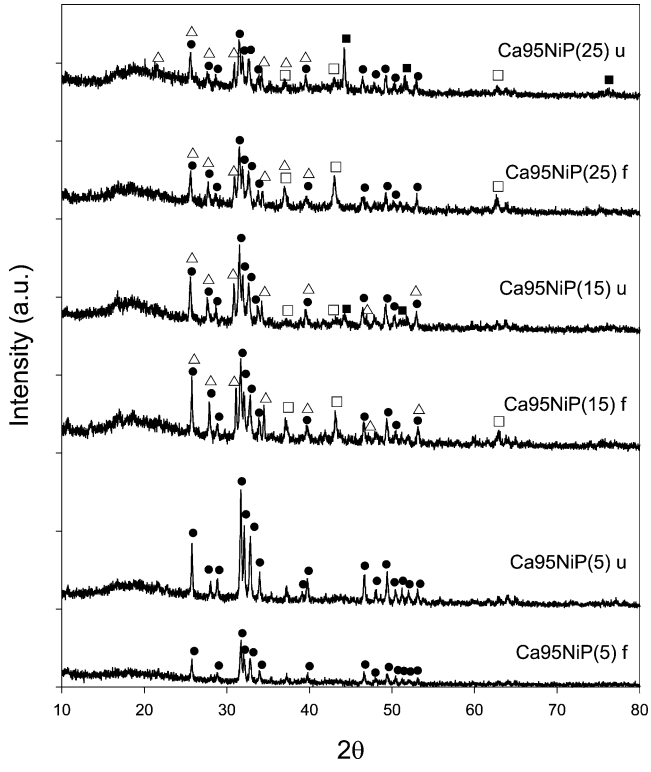

Fig. 4. X-ray diffractograms for Ca95NiP(5), Ca95NiP(15), and Ca95NiP(25) (△, β-$Ca_3(PO_4)_2$; ●, $Ca_{10}(PO_4)_6(OH)_2$; □, NiO; ■, Ni).

This suggests that it is highly probable that a part of the nickel (as Ni^{2+}) may incorporate into the phosphate structure by taking the position of Ca^{2+} [19]. In the catalyst with a low content of Ni such as Ca80NiP(5), NiO phase was hardly observed. This may be due to the small amount of the nickel or some of the nickel taking the position of the calcium. In the catalyst with a higher content of nickel such as Ca80NiP(15), the NiO phase was present in the fresh sample but it was barely seen. In the used Ca80NiP(15), the NiO and metallic Ni phases were hardly seen. As the nickel content increased further, the amount of the NiO phase in the fresh catalyst increased. In Ca80NiP(30) having the highest nickel content among the Ca80NiP(a) catalysts investigated (ca. 16.0 wt% Ni), the amount of NiO in the fresh sample was quite large. In the used Ca80NiP(30), the NiO almost disappeared but the metallic nickel was observed in almost the same amount of NiO in the fresh sample. This tells us that most of the NiO can be reduced to the metallic state during the reaction. Moreover, a considerable portion of the metallic nickel remained not reoxidized even if the used sample had been exposed to flowing CH_4–O_2 at 673 K for 1 h.

Fig. 3 shows XRD patterns for some samples of Ca85NiP(a) catalysts. For the catalyst with a low content of Ni such as Ca85NiP(5), the phosphate was the dominant phase and only a small amount of the apatite was observed. Although the Ca/PO_4 mole ratio employed, 8.5/6, is lower than 10/6, the presence of the apatite phase indicates that a part of the Ni may be incorporated into the apatite structure. The presence of NiO or metallic Ni phase was not clearly seen and the presence of nickel phosphate was not observed. In the catalyst with a higher content of Ni such as Ca85NiP(15), in contrast to Ca80NiP(a) and Ca85NiP(5), both the phosphate and the apatite phases were present in comparable amounts. In the fresh Ca85NiP(15), the presence of a significant amount of NiO was observed. In the used Ca85NiP(15), the presence of metallic Ni was observed while the amount of NiO was considerably decreased when compared with that in the fresh sample. In the catalyst with a higher content of Ni such as Ca85NiP(25), the phosphate became again the dominant phase while the apatite phase was present in a very small amount. The amount of NiO in the fresh sample was large but in the used catalyst it became smaller with the appearance of the metallic Ni. Despite the high content of Ni, especially when the $(Ca + Ni)/PO_4$ ratio is higher than 10/6, dominance of the phosphate phase suggests that Ni species may be apt to get together by themselves rather than to incorporate into the apatite or phosphate structure, thus to form large NiO particles. The NiO in the fresh samples is reduced to the metallic Ni under the reaction conditions that provide a reducing environment by the presence of H_2, CO, and CH_4.

Belik et al. [19] have recently reported that the Sr–Fe(or Ni)–PO_4 system exists as a single phase, as a mixture of multiple phases, or as a solid solution of 2–4 phases, depending on the composition. For example, $SrFe_2(PO_4)_2$ and $Sr_9Fe_{1.5}(PO_4)_7$ form a single phase. For the $Sr_{3-x}Fe_x(PO_4)_2$ system in the $0.34 \leqslant x \leqslant 0.43$ range, there exist the $Sr_3(PO_4)_2$ phase and a solid solution of $Sr_9Fe_{1.5}(PO_4)_7$ and $SrFe_2(PO_4)_2$. They also showed that Ni, Co, Cu, Zn, Mn, and Cd could substitute the Sr^{2+}. The $Sr_{3-x}Ni_x(PO_4)_2$ system exists as a solid solution of $Sr_2Ni(PO_4)_2$ and $Sr_9Ni_{1.5}(PO_4)_7$ in the $0.32 \leqslant x \leqslant 0.39$ range. This tells us that the nickel can substitute or take the position of Ca^{2+} in the phosphate and the apatite structure. In addition, this may also be applicable to the explanation of complicated constitution of the phosphate and apatite phases depending on the composition.

The XRD patterns of some samples of Ca95NiP(a) catalysts are shown in Fig. 4. In these catalysts the apatite phase was the dominant phase, which is different from the results for Ca80NiP(a) and Ca85NiP(a) catalysts. This is certainly due to the higher Ca/PO_4 ratio, which is favorable for the formation of the apatite phase. In Ca95NiP(5), the phosphate phase was not seen, and the NiO phase was hardly observed because the Ni content was low. In the catalysts with higher contents of Ni such as Ca95NiP(15) and Ca95NiP(25), the phosphate phase was present in a significant amount, although it was considerably smaller than the apatite phase. Metallic Ni species was observed in the used catalysts and its amount appeared to increase with the Ni content. For Ca90NiP(a) catalysts (not shown for brevity's sake), the XRD patterns were somewhere in the midway of Ca85NiP(a) and Ca95NiP(a) catalysts.

For Ca100NiP(a) catalysts, the apatite was the dominant phase while the phosphate was present in very small amounts (Fig. 5). Because the $(Ca + Ni)/PO_4$ mole ratio

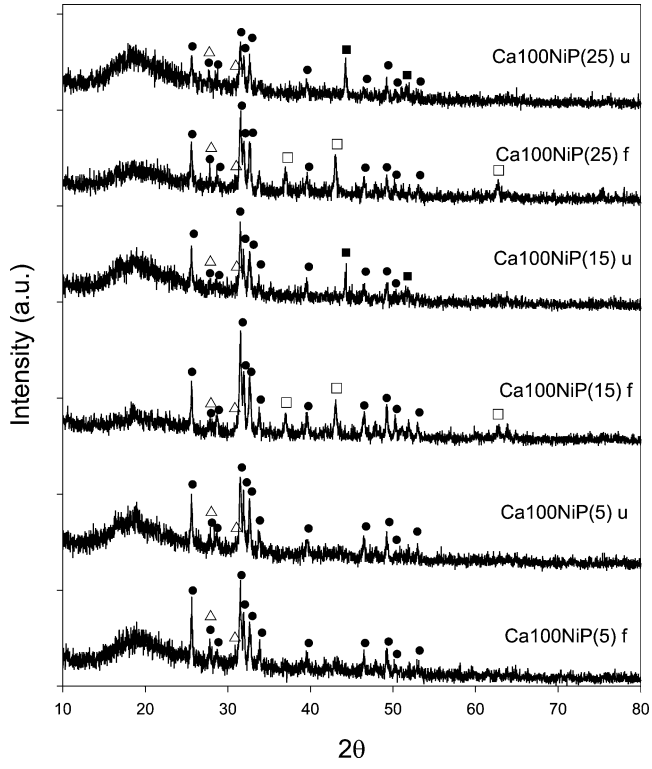

Fig. 5. X-ray diffractograms for Ca100NiP(5), Ca100NiP(15), and Ca100NiP(25) (△, β-$Ca_3(PO_4)_2$; ●, $Ca_{10}(PO_4)_6(OH)_2$; □, NiO; ■, Ni).

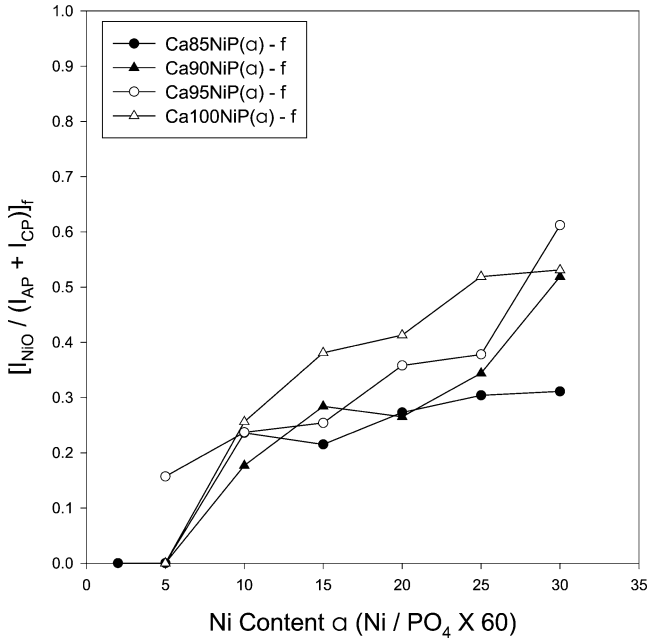

Fig. 6. Relative peak intensities of NiO with respect to the sum of calcium phosphate and apatite peak intensities against the Ni content and Ca/PO_4 ratio for fresh catalysts (the most intense peak for each phase is chosen for comparison).

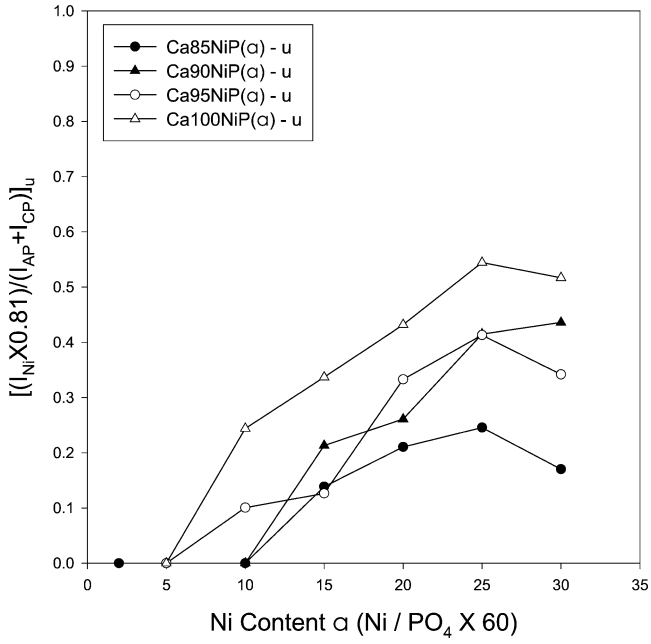

Fig. 7. Relative peak intensities of Ni with respect to the sum of calcium phosphate and apatite peak intensities against the Ni content and Ca/PO_4 ratio for used catalysts (the most intense peak for each phase is chosen for comparison).

employed is considerably higher than 10/6, the apatite phase will be much more favorable to form. As the Ni content increased, the amount of NiO again increased in the fresh catalysts and the amount of metallic nickel also increased in the used catalysts with the decrease of the NiO.

3.2.2. Relative amount of Ni and NiO depending on the Ni content and Ca/PO_4 ratio

From the XRD results, the relative amounts of NiO and Ni depending on the nickel content and the Ca/PO_4 ratio were determined. In the investigated catalysts, the phosphate and apatite phases were present in a mixed state and the ratio of the two phases varied depending on the composition. Nevertheless, the amounts of the phosphate and the apatite in a fresh sample appeared to be nearly the same as those in the corresponding used sample. Therefore, the sum of the main peak intensities of the apatite (211) plane (I_{AP}) and the phosphate ($0.2.\underline{10} + 217$) plane (I_{CP}) was used as the reference for convenience sake since the difference in the Ca/PO_4 ratios in these two phases was small. The ratio of NiO (211) peak intensity (I_{NiO}) to the reference and the ratio of Ni (111) peak intensity multiplied by 0.81 to the reference were obtained in order to determine the relative amounts. The factor of 0.81 means the intensity ratio of NiO (211) peak to Ni (111) peak (or the molar sensitivity ratio of NiO to Ni being $1/1.23 = 0.81$) obtained by calibration for a mixture of the same moles of NiO and Ni.

Fig. 6 shows the relative amount of NiO in the fresh samples. As the nickel content increased, the amount of the NiO increased. As the Ca/PO_4 ratio increased, the amount of the NiO tended to increase. Similar results were obtained for the relative amount of metallic Ni in the used samples (Fig. 7). However, except for Ca90NiP(a) catalysts, the maximum amount of the Ni appeared at the Ni/PO_4 ratio of 2.5/6 for the samples with a fixed ratio of Ca/PO_4. The amount of Ni in the samples with the Ni/PO_4 ratio of 3.0/6 became smaller, and this is considered due to that a significant portion of the NiO, probably that in the core of the large particles, could not be reduced. Actually, the presence of considerable amounts of unreduced NiO was observed in those used samples.

Fig. 8 shows the relative amount of (Ni + NiO) in the used samples. One thing to note here is that the amount of (Ni + NiO) in the used sample was considerably larger compared with the amount of NiO in the fresh sample. This strongly supports the suggestion that in the fresh sample a significant portion of the nickel is taking the position of Ca^{2+} in the phosphate and apatite structures but it comes out of the structures to form metallic nickel particles under reducing environment during the reaction, resulting in more moles of Ni present on the catalyst surface compared with the fresh sample. Another thing to note here is that not all the NiO and metallic Ni particles in the used sample may have been observed by XRD. That is, although a portion of the nickel that had come out of the phosphate and apatite structures might agglomerate and form big particles, a significant portion of the nickel remained as very fine particles smaller than a few nanometers, as observed by HRTEM, and these particles would not have been detected by XRD due to its limitation [20].

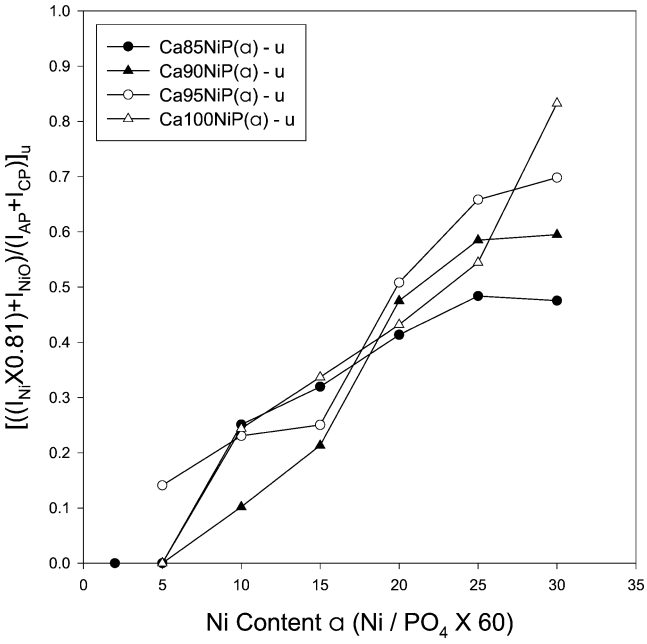

Fig. 8. Relative peak intensities of Ni + NiO with respect to the sum of calcium phosphate and apatite peak intensities against the Ni content and Ca/PO_4 ratio for used catalysts (the most intense peak for each phase is chosen for comparison).

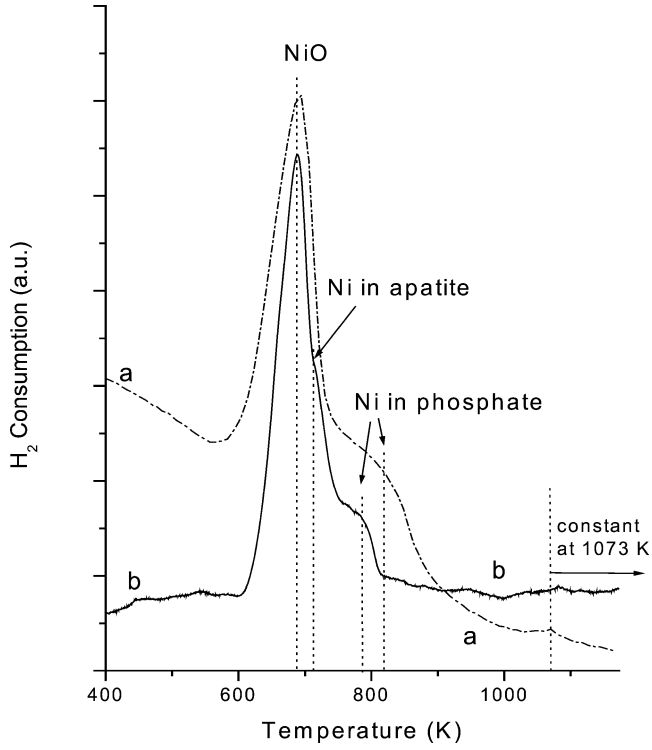

Fig. 9. TPR patterns of (a) Ca85NiP(15) and (b) Ca95NiP(25).

3.3. TPR results

Fig. 9 shows the TPR results for Ca95NiP(25) and Ca85NiP(15). For the Ca95NiP(25), hydrogen consumption started at around 600 K and there appeared at least three peaks. The first peak at around 690 K is considered due to reduction of free NiO, according to earlier works [14,21–23]. The second and third peaks at around 715 and 780 K are attributable to nickel species that are less easily reducible than NiO. One might think that the second peak is attributable to very fine NiO particles that have a stronger interaction with the substrate (apatite and phosphate) than the larger NiO particles. However, since the presence of very fine particles of a few nanometers, especially of the needle shape, in the fresh sample was not observed by HRTEM, this is not considered to be the case. Instead, they may be assigned to the nickel ions substituting Ca^{2+} in the apatite and phosphate structures. Although presence of calcium nickel hydroxyapatite and calcium nickel phosphate, in which a part of Ca^{2+} was substituted with Ni^{2+}, could not be identified by XRD, this does not necessarily rule out their presence if their XRD patterns are almost the same as the calcium hydroxyapatite and the calcium phosphate, respectively (note: there appear no diffraction files for calcium nickel hydroxyapatite and calcium nickel phosphate in JCPDS and no other reports for these phases have not yet been found in the literature). The presence of strontium nickel phosphate in the previous works [17,19] strongly supports the possible presence of the calcium nickel hydroxyapatite and calcium nickel phosphate because the substituting chemistry would be the same (Ca and Ni have the same oxidation number of +2). Therefore, it would be more accurate to consider that the apatite phase actually consists of calcium hydroxyapatite and calcium nickel hydroxyapatite. The phosphate phase would be the same case. The OH–Ni–O–PO_3– structure in the apatite is considered to be chemically less stable than the –PO_3–O–Ni–O–PO_3– structure in the phosphate when comparing the OH–Ni– and –PO_3–O–Ni– structures, and hence the second peak is attributable to the Ni in the former structure. The amount of the free NiO is much larger than the sum of the amounts of the Ni in the apatite and phosphate. The amount of the Ni in the phosphate is larger than that of the apatite, which is consistent with the argument that the nickel in the phosphate structure is more stable. In other words, incorporation of nickel into the phosphate structure is more favorable than into the apatite structure.

For the Ca85NiP(15), two peaks, the first and the third, were clearly observed but the presence of the second peak was not clear. The first peak also appeared at around 690 K again due to the reduction of free NiO. The other peak at around 820 K is also assigned to the nickel ions incorporated into the phosphate structure. In this sample, the nickel ions incorporated into the apatite structure were not clearly observed. This again means that nickel would be more difficult to incorporate into the apatite structure than the phosphate. It would be worthwhile to note that the reduction temperature of the nickel that has a strong interaction with θ-Al_2O_3 has been reported to be 913 K from a TPR study [23], which is considerably higher than the temperature of the above third peak.

Table 1
N_2 physisorption and H_2 chemisorption on fresh catalysts

	Ca95NiP(10)	Ca95NiP(15)	Ca95NiP(20)	Ca95NiP(25)	Ca95NiP(30)
BET surface area of catalyst (m^2/g)	16.8	14.2	18.2	8.6	15.6
Pore volume (cm^3/g)	0.03	0.05	0.05	0.02	0.08
H_2 chemisorption[a] (μmol/g)	4.59	5.44	3.78	2.70	17.0
Exposed of Ni (%)	0.48	0.38	0.21	0.12	0.66
	Ca100NiP(5)	Ca100NiP(15)		Ca100NiP(25)	
H_2 chemisorption[b] (μmol/g)	1.21	1.64		4.26	
Exposed of Ni (%)	0.24	0.12		0.18	

[a] With volumetric adsorption apparatus.
[b] With H_2 pulse experiment.

3.4. Hydrogen chemisorption and oxygen sorption

Hydrogen chemisorption was performed on reduced Ca95NiP(*a*) with Micromeritics ASAP-2000 and on reduced Ca100NiP(*a*) with H_2 pulse chemisorption, as described in Section 2.2 under Experimental. Table 1 shows the hydrogen chemisorption results. The amounts of H_2 chemisorption measured by the volumetric adsorption apparatus ranged from 2.7 to 17.0 μmol/g_{cat} and the percentages exposed of Ni were below 0.7%. These are quite small amounts, almost in the error range of the measurement. Therefore, it was hard to tell any trend with the Ni content. However, when the pulse chemisorption was employed, the amount of H_2 chemisorption tended to increase with the Ni content, although the amounts were very small.

Fig. 10 shows the oxygen pulse sorption results for Ca95NiP(25) and Ca100NiP(*a*). Sorption means here the chemisorption at the surface plus penetration into or oxidation of the bulk nickel. Before oxygen sorption the samples were reduced in hydrogen at 1023 K for 2 h. The molar ratio of total nickel to the total sorbed oxygen atom for Ca100NiP(5) was only 0.19, while that for the other catalysts was similar to each other, ranging from 0.59 to 0.69. The significantly lower ratio for the catalyst with low nickel content is considered due to the reason that most of the nickel would be present in the phosphate and apatite structures and be more stable (more difficult to be reduced) or that the nickel present deep inside the large crystallites would not have the opportunity to contact the H_2 and migrate to the surface. On the contrary, for the catalyst with high nickel content, a significant portion of the nickel in the fresh sample is already present as NiO, probably at the surface, and it would be more easily reducible and sorb oxygen. Moreover, the nickel in the phosphate and apatite structures might be more easily reducible due to the higher extent of the substitution of Ca. The nickel unreduced by the hydrogen treatment may be again due to that present deep inside the large crystallites of NiO, calcium nickel phosphate, and calcium nickel hydroxyapatite. Nevertheless, the portion of reduced nickel was very much higher compared with the percentage exposed of metallic Ni (less than 0.7%) determined by the H_2 chemisorption.

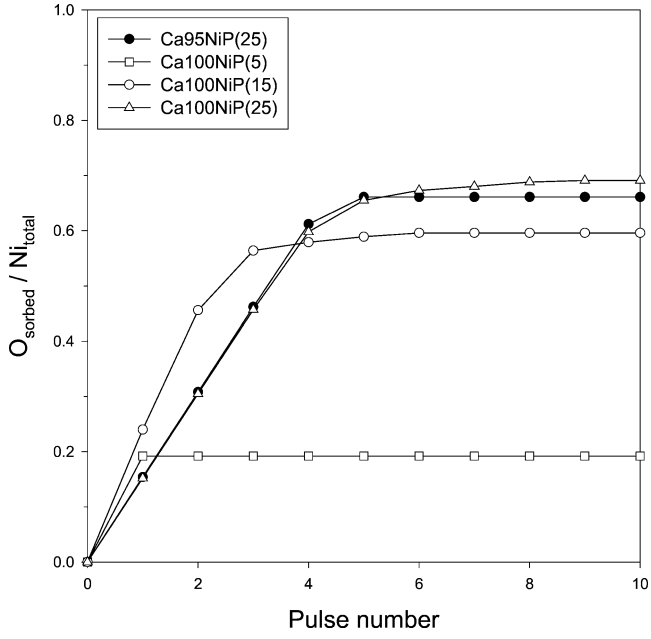

Fig. 10. The O_{sorbed}/Ni_{total} at 923 K vs pulse number over Ca95NiP(25) and Ca100NiP(*a*) reduced at 1023 K.

3.5. XPS analyses

Fig. 11 presents XPS spectra in the Ni 2p region for Ca85NiP(30). Since the samples had been exposed to an oxidizing environment, the presence of metallic nickel (the binding energy (b.e.) = ∼ 852 eV) at the surface could not be expected. The peaks at the b.e. of ∼ 857 and 874 eV are for Ni^{2+} $2p_{3/2}$ and $2p_{1/2}$. The peak at the b.e. of ∼ 862 eV is the shakeup satellite peak [6]. The b.e. of Ni $2p_{3/2}$ in NiO is reported to be ∼ 854 eV, and that in $Ni(OH)_2$, $NiAl_2O_3$, $NiSO_4$, or $NiSiO_3$ to be 856–857 eV [6,24]. Therefore, the peak at the b.e. of ∼ 857 eV is considered to come from Ni^{2+} in the phosphate (P–O–Ni–O–P) or the apatite

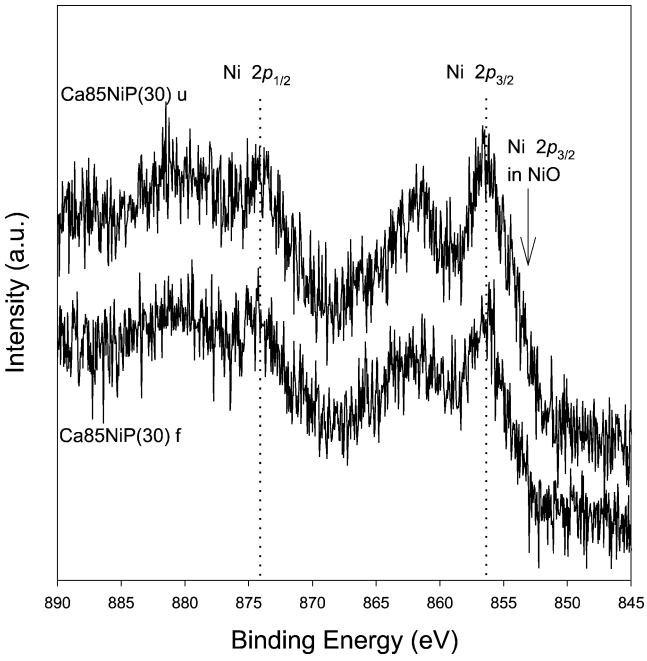

Fig. 11. XPS spectra for Ni 2p region in Ca85NiP(30).

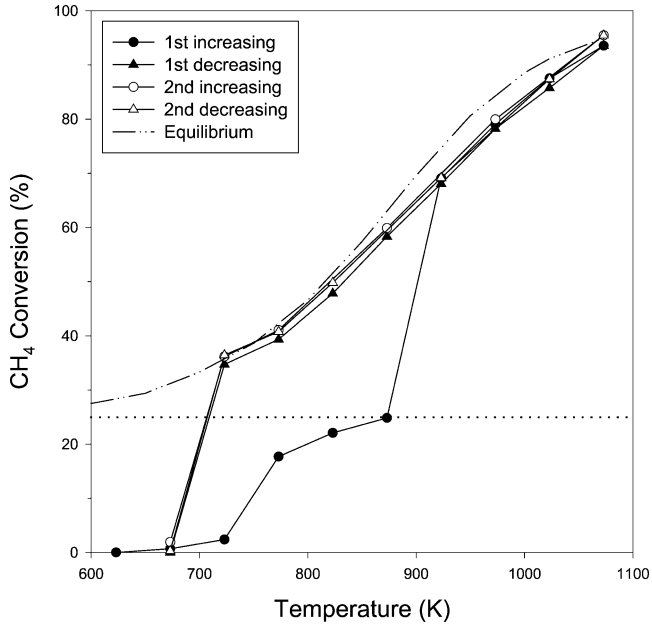

Fig. 12. CH_4 conversion with repeated increasing (●, first; ○, second) and decreasing (▲, first; △, second) temperature over Ca95NiP(25).

(HO–Ni–O–P) structure [16]. This is consistent with the XRD result that the phosphate and the apatite phases were present in fresh Ca85NiP(*a*) catalysts. That is, a part of nickel was incorporated into the phosphate and the apatite structure by taking the position of Ca^{2+}.

Although the presence of large amounts of NiO and metallic Ni was observed by XRD, the presence of NiO at the surface was not clearly seen by XPS and its amount appeared to be small. No significant differences in the XPS spectra were observed between the fresh and used samples even though many fine particles were formed in the used sample. The relatively sharp XRD peak for NiO in the fresh sample represents that most of the NiO particles are large, larger than 100 nm when estimated by the Scherrer equation [20]. As a consequence, the amount of Ni atoms at the surface of large NiO particles could be quite smaller than the amount of Ni atoms at the surface of calcium nickel phosphate and calcium nickel hydroxyapatite. This could be a possible explanation for the small amount of Ni^{2+} with a b.e. of $\sim$ 854 eV compared with that of $\sim$ 857 eV in the fresh sample. For the used sample, the reason for the small amount of Ni^{2+} with a b.e. of $\sim$ 854 eV is hard to understand when considering the fact that many fine particles were formed. However, when the small H_2 chemisorption is taken into account, it is suggested that the fine particles might be covered with, or decorated with, or strongly interact with the phosphate and hydroxyl groups, resulting in a relatively large amount of Ni^{2+} with a b.e. of $\sim$ 857 eV and, at the same time, suppression of H_2 chemisorption. Since the amount of H_2 chemisorption was very small on these catalysts, the H_2 chemisorption method may not be helpful to a study for the change of active metal surface due to sintering or coking. It is notable that the catalysts exhibited excellent catalytic performance (see Section 3.6) despite the low H_2 chemisorption. This is not well understood at present, but this might be another kind of strong-metal-support interaction (SMSI). A more detailed study may be needed in the future.

3.6. Catalyst activation and performance

The POM reaction was carried out by sequentially increasing and decreasing the temperature with 50° intervals, and the results over Ca95NiP(25) are shown in Figs. 12–14. When the temperature was first increased, the activity of the catalyst was very low below 723 K. Up to 873 K, the methane conversion was lower than 25% and CO_2 was practically the sole carbon product; the H_2 yield was only about 0.1%. At 923 K, the methane conversion was about 25% with no CO formation during initial 30 min of time on-stream, but after 1 h the conversion abruptly rose to 69% with CO selectivity of 75%, H_2 yield of 62%, and H_2/CO ratio of 2.8. This indicates that the Ni is reduced to the metallic state at this temperature. Above this, the conversion, CO selectivity, and H_2 yield increased gradually with the temperature, and at 1073 K the conversion of 93%, the CO selectivity of 96%, and the H_2 yield of 90% were obtained. These values are very close to the equilibrium values.

While the temperature was decreased afterward, reproducible results were obtained down to 923 K. Below this, however, the conversion decreased gradually down to 723 K and did not follow the path of the first increasing sequence. At 723 K, the conversion was 35% and the CO selectivity was 9%. At 673 K, the activity dropped to near zero, but it took about an hour to lose the activity completely. When the temperature was increased and decreased again, the results reproducibly followed the path of the first decreasing

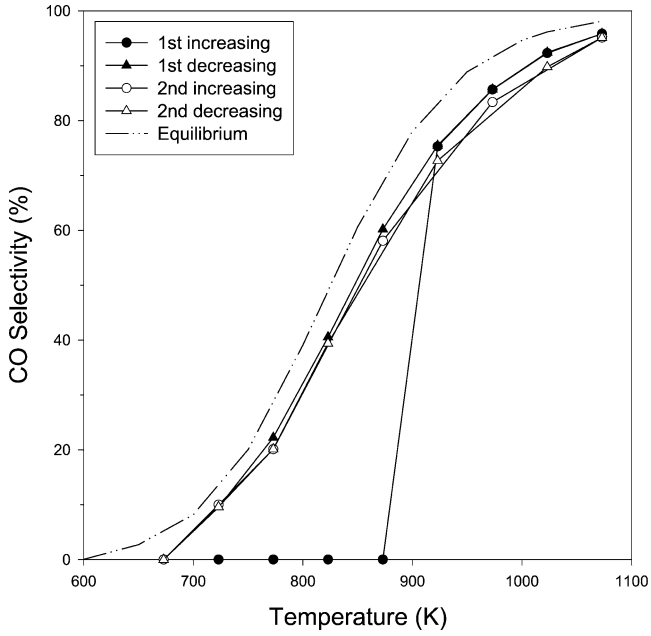

Fig. 13. CO selectivity with repeated increasing (●, first; ○, second) and decreasing (▲, first; △, second) temperature over Ca95NiP(25).

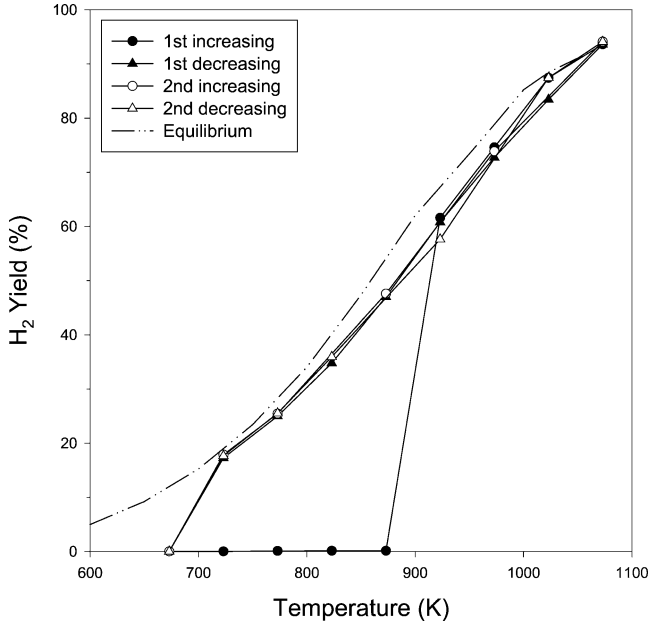

Fig. 14. H_2 yield with repeated increasing (●, first; ○, second) and decreasing (▲, first; △, second) temperature over Ca95NiP(25).

sequence. At 723 K, the activity was readily restored afterward.

The above results can be explained as follows. In the fresh catalyst, all the Ni is present as the oxidized state, and therefore only the completely oxidized products are produced at low temperatures. While the temperature was first increased, it needs higher temperature and more time for the Ni to be reduced when compared with the case of H_2 being used as the reducing agent, because the CH_4–O_2 mixture is a weaker reducing agent than H_2. This is well explained by the fact that

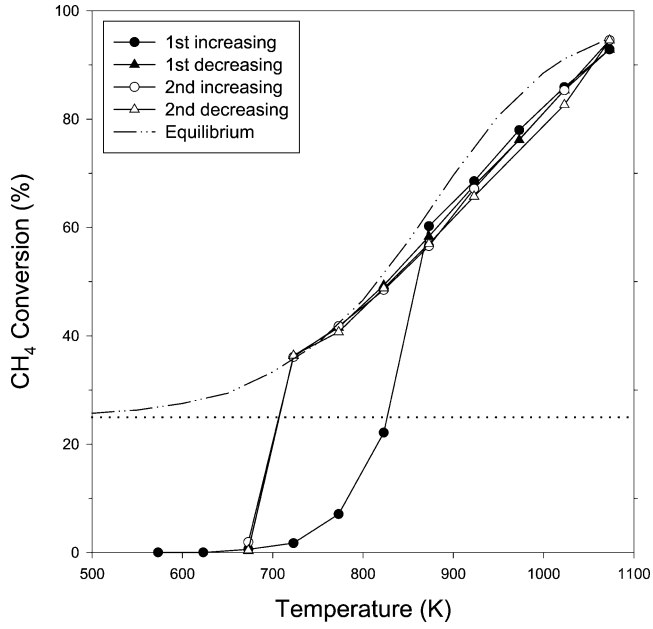

Fig. 15. CH_4 conversion with repeated increasing (●, first; ○, second) and decreasing (▲, first; △, second) temperature over Ca90NiP(20).

it takes about 1 h at 923 K for the catalyst to exert its full potential. At 923 K during the first temperature increase, the Ni in the phosphate and apatite structures is considered to come out and reduce to the metallic Ni state, as is evidenced by the TPR results. Once a part of the Ni is reduced, CO and H_2 concentrations become higher and reduction of the Ni can be accelerated. While the temperature is decreased, it is believed that the Ni is progressively oxidized. Eventually at a certain low temperature, 673 K, the surface of Ni particles is all oxidized and exhibits no POM activity, but the Ni in the core of the particles still remains as the metallic state, as evidenced by the XRD data. When the temperature was increased afterward, the activity can be restored more easily at 723 K since the Ni surface was covered only with a thin layer of oxidized nickel that is more readily reducible. This activation temperature of 723 K is a little higher than the reduction temperature of NiO under hydrogen environment, 680 K.

Similar results were observed for other catalysts (Figs. 15–16). During the first-increasing sequence, Ca85NiP(15) exhibited the sudden increase of the activity at 723 K while Ca90NiP(20) did at 873 K. Nevertheless, they all lost the POM activity at 673 K. For Ca85NiP(15), the first activation temperature was so low that the hysteresis was exceptionally not observed between the temperature increasing and decreasing sequences.

The first activation temperature of Ca85NiP(25) was 973 K (Fig. 17). This temperature is higher than that of Ca85NiP(15) with the same Ca/PO_4 ratio. This may be partly explained by the TPR and XRD results. In the XRD results, two samples had similar amounts of the NiO phase. However, while similar amounts of the apatite and phosphate phases were present in Ca85NiP(15), the phosphate

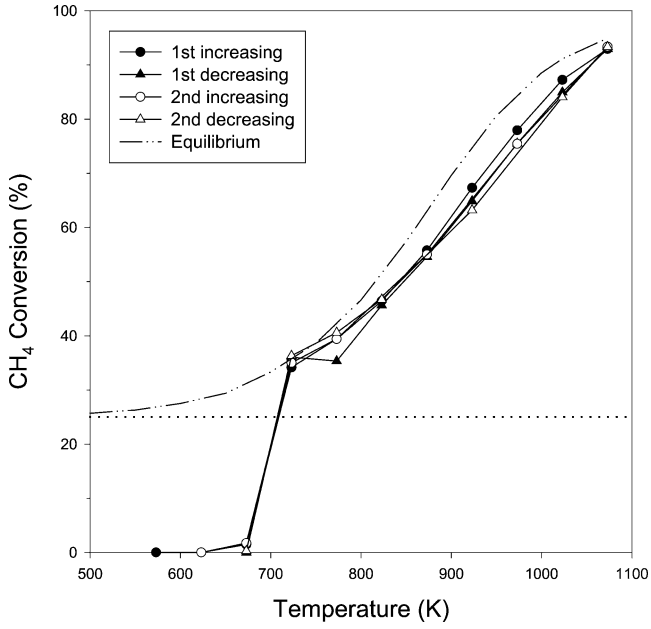

Fig. 16. CH_4 conversion with repeated increasing (●, first; ○, second) and decreasing (▲, first; △, second) temperature over Ca85NiP(15).

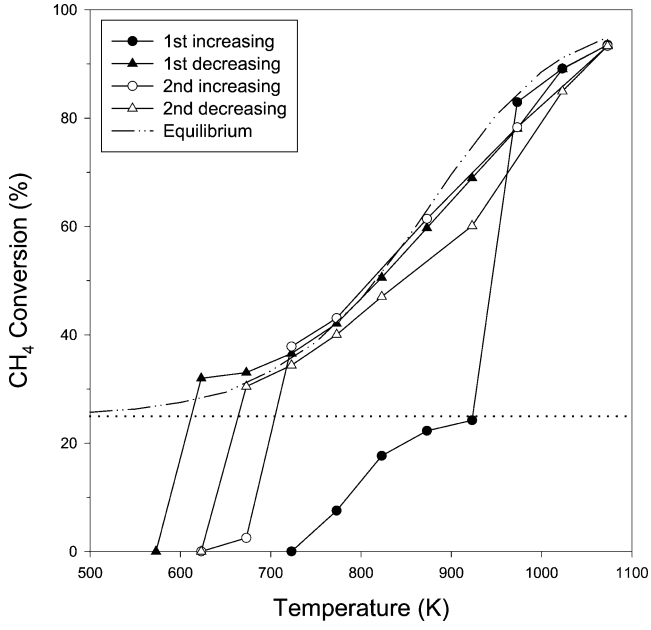

Fig. 17. CH_4 conversion with repeated increasing (●, first; ○, second) and decreasing (▲, first; △, second) temperature over Ca85NiP(15).

phase was dominant in Ca85NiP(25). As noted in the TPR results, NiO was the most easily reducible, the Ni incorporated in the apatite was the next, and that in the phosphate was the most difficult to reduce. Therefore, the nickel of Ca85NiP(15) could be reduced at a lower temperature than that of Ca85NiP(25). The first activation temperature of Ca95NiP(25), 923 K, is lower than that of Ca85NiP(25) but higher than that of Ca85NiP(15). This suggests that the ratio of the apatite to the phosphate does not seem to be determinative for the first activation temperature but partly influential. Other factors, such as the nickel content, may be operative. In this case, as the nickel content becomes higher, it appears that the first activation temperature gets higher.

Sometimes when the temperature decreased, the activity did not drop abruptly at 673 K but sustained considerably high down to about 600 K or below, as shown in Fig. 17. However, this was not reproducible but the temperature of sudden activity drop appeared irregular. This phenomenon is considered due to the exothermic nature of the oxidation reactions, resulting in a behavior of an autothermal reaction or presence of hot spots as reported by Dissanayake et al. [6]. A further study may be needed to better understand this.

The hysteresis of the activity and selectivity observed in the first cycle of temperature increasing–decreasing sequence has also been observed similarly in other catalysts such as oxide-supported Ni catalysts [5,6,11] and Ni-strontium phosphate catalysts [16]. For these catalysts, the hysteresis was repeatedly observed in subsequent cycles. Although some experimental conditions in those works and in this work are different, especially as to the space velocity and partial pressures of methane and oxygen in the feed (Table 2), the common results are as follows: at the lower branch, where the methane conversion does not exceed 25% (the maximum conversion when only the complete oxidation occurs with a CH_4/O_2 feed ratio of 2), CO_2 and H_2O are the sole products; at the temperature-decreasing branch, the O_2 conversion was virtually 100%. The differences are the temperatures at which the sudden increase and decrease in the methane conversion occur. Below 673 K, all the catalysts lose the POM activity anyway.

Dissanayake et al. [5] as well as van Looij and Geus [11] explained about the hysteresis as follows. At the temperature-increasing branch, the nickel is initially present as an oxidized state, yielding completely oxidized products, but at a certain high temperature it is reduced rapidly by H_2, CO, or CH_4 to the metallic state, giving partially oxidized products. Upon decreasing the temperature, the metallic nickel in gradually oxidized, and eventually the metallic nickel is all reoxidized by the O_2 at a certain low temperature. The main point is that metallic nickel is the active and effective component for the selective partial oxidation of methane. The same explanation may be applicable to the catalysts in this work.

Comparison of the catalysts in this work and the other catalysts is summarized in Table 2. For the catalysts in this work, however, the hysteresis was not observed any more in the subsequent cycles, and this is a salient difference of the Ni–calcium phosphate/hydroxyapatite catalysts from the other Ni catalysts noted above, besides the activation temperature being relatively lower. This suggests that the Ni–calcium phosphate/hydroxyapatite catalysts are more easily reducible than the other Ni catalysts. This may be attributed to the absence of the oxide support or to a weaker metal–support interaction compared with the oxide support. Actually, even after the used catalyst was exposed to ambient air

Table 2
Comparison of activation temperature and reaction conditions employed with increasing–decreasing temperature sequences for various Ni catalysts

Catalyst	Catalyst charge	P_{CH_4} (atm)	P_{O_2} (atm)	Total flow rate (cm^3/min)	First activation temp. (K)	Reference
Ca85NiP(15)	0.2 g	0.16	0.08	100	723	This work
Ca90NiP(20)	0.2 g	0.16	0.08	100	873	This work
Ca95NiP(25)	0.2 g	0.16	0.08	100	923	This work
	0.5 g				973	
Ca85NiP(25)	0.2 g	0.16	0.08	100	973	This work
$Sr_{9.0}Ni_{1.0}(PO_4)_6$	0.2 g	0.16	0.08	100	1023	[16]
	0.5 g				973	
	1.0 g				873	
25 wt% NiO/SiO_2	50 mg	0.01	0.005	100	1050	[11]
25 wt% NiO/Al_2O_3–TiO_2–CaO	50 mg	0.064	0.036	50	1023	[5]

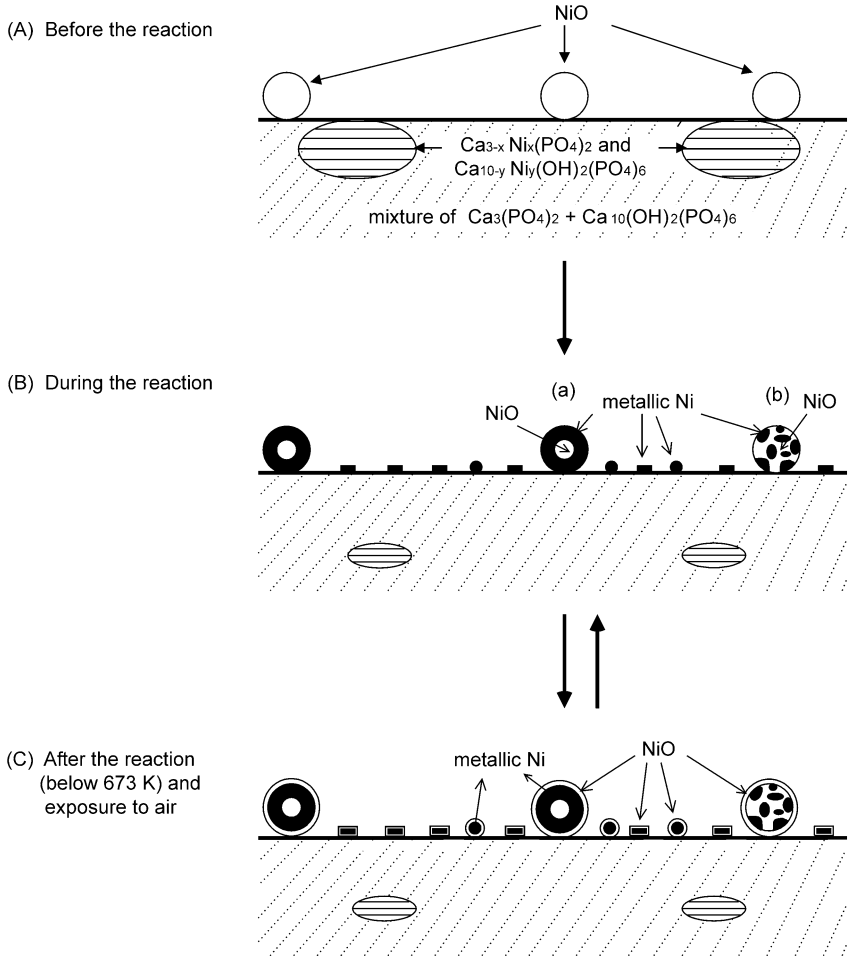

Fig. 18. Proposed scheme of changes of Ni state in POM reaction.

overnight, it was found that it could be reactivated at 723 K under the standard reaction conditions.

3.7. Proposal for changes of the nickel state

Fig. 18 shows the process for changes of the nickel state based on the above discussion. Before the reaction, the catalyst exists in a mixed state of calcium phosphate, calcium hydroxyapatite, calcium nickel phosphate, calcium nickel hydroxyapatite, and NiO; the NiO particles probably lay on the surface (Fig. 18A). As the reaction temperature increases and reaches a certain temperature, the NiO is reduced from the outside (Fig. 18B,a) or through the cracks in the crystallite (Fig. 18B,b) under reducing environment that is provided by the consumption of O_2 and the production of H_2 and CO. The nickel in the phosphate and apatite structures gradually comes out and forms fine particles and is reduced, which is evidenced by the TPR, TEM, and activation experi-

ments. Upon decreasing the temperature, the catalyst surface is gradually reoxidized. Finally, at 673 K or below, the metallic nickel surface is completely covered with a thin layer of oxygen, NiO (Fig. 18C), but the nickel that has come out does not go back to the phosphate or the apatite structure. When the temperature is increased again, it returns to the B state. This cycle can be repeated while the temperature is decreased and increased.

4. Conclusions

Nickel–calcium phosphate/hydroxyapatite, a new type of catalyst with no oxide support, exhibited excellent performance for the partial oxidation of methane, yielding values close to the equilibrium. This material, if activated once, could be activated at 723 K after total reoxidation of the nickel surface without employing the H_2 pretreatment but with CH_4–O_2 only. This may be due to the absence of the oxide support and thin layers of NiO at the particle surface formed during the reoxidation. At least three nickel species were present in the fresh sample and the crystalline phases were calcium phosphate, calcium hydroxyapatite, calcium nickel phosphate, calcium nickel hydroxyapatite, and NiO. As the Ca/PO_4 ratio increased, the amount of the apatite phase became larger. As the Ni/PO_4 ratio increase, the amount of NiO in the fresh catalyst became larger. In the used catalysts, the metallic Ni was observed with significant decrease of the NiO. TEM showed that many fine nickel particles of a few nanometers in needle and round shapes that had not been observed in the fresh sample were present in the used sample. These are believed to be formed from the nickel that has come out of the calcium nickel phosphate and calcium nickel hydroxyapatite under reducing environment during the reaction. Therefore, most of the catalytic activity was attributed to the fine Ni metal particles. The amount of H_2 chemisorption was very small (the percentage exposed of $Ni < 1\%$) while the amount of O_2 sorption was quite large ($O_{sorb}/Ni_{total} \sim 0.6$). The suppression of H_2 chemisorption might be attributed to the covering of the nickel particles with the phosphate and/or hydroxyl groups or to a strong interaction with those groups.

References

[1] C.T. Au, H.Y. Wang, J. Catal. 167 (1997) 337.
[2] Y. Chen, C. Hu, M. Gong, Y. Chen, A. Tian, Stud. Surf. Sci. Catal. 130 (2000) 2543.
[3] V.R. Choudhary, B.S. Uphade, A.S. Mamman, J. Catal. 172 (1997) 281.
[4] A.M. Diskin, R.M. Ormerod, Stud. Surf. Sci. Catal. 130 (2000) 3519.
[5] D. Dissanayake, M.P. Rosynek, K.C.C. Kharas, J.H. Lunsford, J. Catal. 132 (1991) 117.
[6] D. Dissanayake, M.P. Rosynek, J.H. Lunsford, J. Phys. Chem. 97 (1993) 3644.
[7] T. Hayakawa, H. Harihara, A.G. Anderson, K. Suzuki, H. Yasuda, T. Tsunoda, S. Hamakawa, A.P.E. York, Y.S. Yoon, Appl. Catal. A 149 (1997) 391.
[8] S. Liu, G. Xiong, H. Dong, W. Yang, S. Sheng, W. Chu, Z. Yu, Stud. Surf. Sci. Catal. 130 (2000) 3567.
[9] K. Takehira, T. Shishido, M. Kondo, R. Furukawa, E. Tanabe, K. Ito, S. Hamakawa, T. Hayakawa, Stud. Surf. Sci. Catal. 130 (2000) 3525.
[10] P.M. Torniainen, X. Chu, L.D. Schmidt, J. Catal. 146 (1994) 1.
[11] F. van Looij, J.W. Geus, J. Catal. 168 (1997) 154.
[12] K. Takehira, from AISTI, Sinotech, Information on New Technology, http://www.mri.co.kr (Oct. 2002).
[13] Z.-W. Liu, K.-W. Jun, H.-S. Roh, S.-E. Park, Y.-S. Oh, Korean J. Chem. Eng. 19 (2002) 735.
[14] Z.-W. Liu, H.-S. Roh, K.-W. Jun, S.-E. Park, T.-Y. Song, Korean J. Chem. Eng. 19 (2002) 742.
[15] S.-H. Lee, K.J. Yoon, Korean J. Chem. Eng. 18 (2001) 228.
[16] S.J. Lee, J.H. Jun, S.-H. Lee, K.J. Yoon, T.H. Lim, S.-W. Nam, S.-A. Hong, Appl. Catal. A 230 (2002) 61.
[17] J.H. Jun, S.J. Lee, S.-H. Lee, T.-J. Lee, S.J. Kong, T.H. Lim, S.-W. Nam, S.-A. Hong, K.J. Yoon, Korean J. Chem. Eng. 20 (2003), in press.
[18] V.R. Choudhary, A.M. Rajput, B. Prabhakar, J. Catal. 139 (1993) 326.
[19] A.A. Belik, B.I. Lazoryak, K.V. Pokholok, T.P. Terekhina, I.A. Leonidov, E.B. Mitberg, V.V. Karelina, D.G. Kellerman, J. Solid State Chem. 162 (2001) 113.
[20] B.D. Cullity, in: Elements of X-Ray Diffraction, 2nd ed., Addison–Wesley, Menlo Park, CA, 1978, pp. 284–285.
[21] W.-S. Dong, K.-W. Jun, H.-S. Roh, Z.-W. Liu, S.-E. Park, Catal. Lett. 78 (2002) 215.
[22] H.-S. Roh, K.-W. Jun, W.-S. Dong, S.-E. Park, Y.-S. Baek, Catal. Lett. 74 (2001) 31.
[23] H.-S. Roh, K.-W. Jun, W.-S. Dong, S.-E. Park, Y.-I. Joe, Chem. Lett. (2001) 666.
[24] D. Briggs, M.P. Seah (Eds.), Practical Surface Analysis: Auger and X-Ray Photoelectron Spectroscopy, Vol. 1, 2nd ed., Wiley, New York, 1990, App.5.